Surface & Coatings Technology 375 (2019) 8–14

Contents lists available at ScienceDirect

Surface & Coatings Technology

journal homepage: www.elsevier.com/locate/surfcoat

Modelling the interaction between bacterial cells and laser-textured surfaces

G. Lazzini[a,*], L. Romoli[a], A.H.A. Lutey[a], F. Fuso[b,c]

[a] Department of Engineering and Architecture, University of Parma, 43124 Parma, Italy
[b] Dipartimento di Fisica Enrico Fermi, Università di Pisa, 56127 Pisa, Italy
[c] INO-CNR, 56127 Pisa, Italy

ARTICLE INFO

Keywords:
Laser
Topography
Antibacterial properties

ABSTRACT

The influence of surface topography resulting from ultrashort pulsed laser texturing on bacterial cell adhesion is studied as a method for preventing contamination on stainless steel components. The initial adhesion of a single spherical cell on a rough surface prior to the onset of any chemical or biological effect is simulated with a numerical approach including non-covalent interactions between the cell and textured substrate. The study demonstrates that when asperities are large enough to allow the cell to occupy valleys between two adjacent protrusions, the cell is protected from hydrodynamic turbulence and is therefore more prone to adhere to the substrate. Results pave the way to validating, in quantitative terms, hypotheses relating to the influence of surface topography on bacterial growth. Two different levels of anisotropy are taken into account to contrast the high adaptability of spherical cells, demonstrating that laser texturing can invoke a specific biological response.

1. Introduction

The requirement to avoid the formation of surface biofilms in food and medical applications has pushed researchers to find new and increasingly more effective surface treatments to inhibit the proliferation of bacterial cells. Common solutions to inhibiting bacterial contamination of surfaces involve the use of antibiotics [1] or the emission of ions [2] such as silver. These techniques have been adopted in biomedical devices such as prosthetic implants for years to contrast the problem of post-surgical nosocomial infections [3]. The side effects produced by such substances and the spread of antibiotic-resistant bacterial strains, however, is pushing researchers to find new solutions to increase the durability and reliability of such devices. In the food production industry, the requirement to ensure adequate levels of hygiene in machinery requires expensive cleaning procedures employing aggressive chemicals and, in most cases, temporary interruptions to the production cycle [4]. To overcome such difficulties, new strategies are being developed to increase the cleanability of such components.

One of the most promising lines of research in this direction is based on the idea of reducing adhesion strength between bacterial cells and a substrate by tailoring the surface roughness [5,6]. Within this context, several surface treatments have proven to be effective in reducing the amount of biofilm compared to untreated surfaces [7,8]. Amongst these techniques, ultrashort pulsed laser texturing has emerged as a powerful and versatile surface engineering process for achieving antibacterial properties [9]. Laser technology is a highly valid approach across a wide range of manufacturing applications due to its simplicity, the absence of requirements for clean room facilities and the possibility of performing the treatment in air or other gaseous environments [9–12]. The ease with which this approach can be applied compared to other surface texturing techniques such as ion beam structuring [13] therefore makes it a good candidate for implementation in an industrial context for processing of large areas.

Laser interaction with metals on a time-scale shorter than the electron-phonon relaxation time leads to a complex array of physical phenomena that depend on the laser wavelength, pulse duration and pulse fluence. Within specific parameter windows, interaction between the incident laser pulse and surface plasmon polaritons leads to the formation of Laser Induced Periodic Surface Structures (LIPSS), elongated ridges perpendicular to the polarisation direction with a separation distance similar to, or smaller than, the laser wavelength [14]. Structures of this type produced with a laser wavelength of 1030 nm have been shown to reduce *Escherichia coli* (*E. coli*) retention by more than 99% and *Staphylococcus aureus* (*S. aureus*) retention by more than 80% compared to reference samples representing current best practise in the food production industry [8]. When considering the interaction of bacterial cells with a textured surface, it must be noted that *E. coli* and *S. aureus* have different geometry; the former is a rod-like cell with a mean base diameter of 1 μm and a length of 2–3 μm [15], while the latter is a spherical cell with a diameter of 0.5–1 μm [16]. Other laser-

* Corresponding author.
E-mail address: gianmarco.lazzini@unipr.it (G. Lazzini).

https://doi.org/10.1016/j.surfcoat.2019.06.078
Received 5 April 2019; Received in revised form 24 June 2019; Accepted 26 June 2019
Available online 27 June 2019
0257-8972/

based techniques such as Direct Light Interference Patterning (DLIP) can also be employed to achieve similar-sized structures that have been shown to reduce bacterial attachment [17–19].

Bacterial adhesion at a single-cell level and the eventual formation of biofilm are complicated processes involving a wide range of physical, chemical and biological phenomena [20]. In particular, local hydrodynamic effects induced by surface topography can influence the probability of irreversible bacterial attachment, the first stage of biofilm growth.

The most widely accepted hypothesis relating to the influence of surface topography on bacterial attachment [21] currently states that surface protrusions whose size are slightly smaller than the bacterial cell size are most effective at reducing the contact area between the cell and substrate by creating a “fakir effect” and thus an unfavourable environment for proliferation. Furthermore, it has been hypothesised that such protrusions could produce local mechanical stresses in the bacterial cell wall that induce alterations in cellular metabolism [22]. The connection between surface topography and bacterial adhesion is reflected in current industrial standards for surface roughness in the food industry ($R_a \leq 0.8$ μm) [23] and length-scale thresholds for the formation of the dental plaque [24]. The principle has also been used to explain the antibacterial nature of several biological interfaces such as gecko's feets or cicada's wings [25–27]. Ultrashort pulsed laser treatment is a good candidate for the production of man-made antibacterial surfaces as it can be used to produce textures with protrusions whose sizes are compatible with the aforementioned requirements.

Such a framework, however, is based on the implicit assumption that a bacterial cell is a perfectly rigid body that interacts with a surface via contact only. Previous studies instead suggest that the problem of bacterial adhesion is more complicated as it is influenced by a range of other physical and chemical factors. Bacterial adhesion is often described as a two-stage process. In the first stage, the cell is kept in the proximity of the substrate by non-covalent interactions including attractive Lifshitz-van der Waals interactions, acid-base interactions, electric double-layer repulsions etc. If the first step takes place, the cell begins to produce extracellular polymeric substances to increase the bonding energy with the substrate. Such behaviour can be influenced by the presence of organic conditioning films on the surface. Furthermore, the role of the liquid environment where the cell is inherently placed is completely excluded from this line of reasoning. In particular, the effects of shear flow or other hydrodynamic mechanisms are not considered, despite occurring in many practical applications such as the food industry.

In an attempt to enable a more realistic description of the initial stages of interaction between a single bacterial cell and a rough laser-textured surface, a novel numerical simulation of cell dynamics in close proximity to a rigid, rough surface will be presented in this paper. In order to isolate hydrodynamic effects, the simplest possible bacterial shape has been considered as a first step, with simulations performed on a single spherical coccoid-like cell whose mechanical properties pertaining to deformation have been modelled based on data from the literature. Cell dynamics have been simulated in the presence of a moving fluid and different substrate topographies inspired by laser-textured surfaces featuring LIPSS in the form of either elongated ripples or isolated dots [28]. Owing to the high flexibility of currently available surface texturing processes in terms of shape, size and aspect ratio, other quasi-regular geometries have also been simulated with the aim of initiating systematic analysis of cell-surface interactions as a function of straightforward geometric parameters such as the ratio of bacterial cell size to surface periodicity or surface structure height.

2. Simulation

Simulations were performed by implementing the *object-in-fluid* feature [29] of the ESPResSo package [30] in a Python code specifically developed to describe motion of a single bacterial cell in close proximity to a textured surface. ESPResSo allows representation of deformable objects as triangular meshes immersed in a fluid, modelled according to the Lattice-Boltzmann algorithm. This computational approach calculates the velocity field of a fluid based on the corresponding Boltzmann distribution determined at the nodes of a simple cubic lattice. The mesh employed to represent the cell was obtained with an icosahedral sphere typically having 642 nodes. Cell nodes interact with each other via bonding forces described through various associated terms such as stretching, bending and so on. By observing the analytical expressions for forces acting on each node, it is possible to note that the dominant contribution to cellular bonding energy for a bacterial cell is given by the so-called stretching interaction, simulated by the presence of a spring along each edge connecting adjacent mesh nodes, and the so-called bending interaction, which takes into account effects produced by variation of the angle between two mesh faces having one edge in common. Explicit expressions for the relevant contributions are given below.

Let L_{AB} be the length of a single mesh edge whose vertices are A and B, and $L_{AB}{}^0$ be the corresponding value in the equilibrium configuration. The stretching contribution to bonding forces is defined as:

$$F_s(A,B) = k_S \kappa\left(\frac{L_{AB}}{L^0_{AB}}\right)\frac{L_{AB}-L^0_{AB}}{L^0_{AB}} n_{AB} \tag{1}$$

where k_S is the stretching force constant, $\kappa(\lambda) = \frac{\lambda^{0.5}+\lambda^{-2.5}}{\lambda+\lambda^{-3}}$, and n_{AB} is the unit vector from A to B (see Fig. 1(a)).

Let θ be the angle between two mesh triangles with a common edge AB, and θ^0 be the corresponding value in the equilibrium configuration. The bending contribution to the bonding forces on vertex C is given by:

$$F_b(ABC) = k_b \frac{\Delta\theta}{\theta^0} n_{ABC} \tag{2}$$

where k_b is the bending force constant, $\Delta\theta = \theta - \theta^0$ is the deviation of

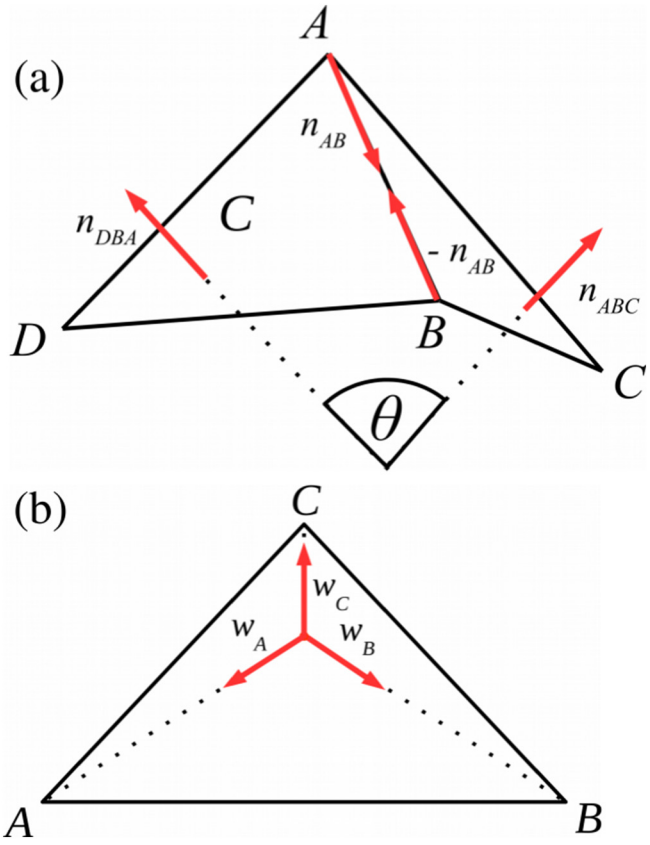

Fig. 1. Representation of geometric quantities relating to stretching, bending and constant-volume interactions (a) and constant-area interactions (b).

θ from the equilibrium value and n_{ABC} is the normal unit vector to the triangle *ABC*. Although stretching and bending terms constitute the dominant contributions, additional forces were included to account for area and volume conservation constraints. The area conservation contribution acting on vertex *A* is given by

$$F_a(A) = -\left(k_{al}\frac{\Delta S_{\mathrm{ABC}}}{S_{\mathrm{ABC}}} + k_{ag}\frac{\Delta S}{S}\right)w_A \tag{3}$$

where k_{al} and k_{ag} are force constants and w_A is the unit vector pointing from the barycentric coordinate of the triangle *ABC* to vertex *A* (see Fig. 1(b)). The first term in brackets takes into account local area conservation and depends on the areal variation $\frac{\Delta S_{\mathrm{ABC}}}{S_{\mathrm{ABC}}}$ of triangle *ABC* with respect to the equilibrium value S_{ABC}. The second term instead considers global area conservation and takes into account the total mesh surface *S*. The total force $F_a(A)$ acting on vertex *A* and due to triangle *ABC* is directed along unit vector w_A, pointing from the centroid of the triangle to point *A*. Finally, volume conservation is given by

$$F_v(A) = -k_v\frac{\Delta S}{S}S_{ABC}n_{ABC} \tag{4}$$

where k_v is the volume force constant.

Values employed for parameters given in Eqs. (1)–(4) were based on data from the literature [31] relating to the stiffness and Young's modulus of *S. aureus*. The corresponding force constants in molecular dynamics (MD) units used by the software are listed in Table 1.

As mentioned above, the mesh representing the cell was immersed in a fluid. The traditional approach for implementing "immersed boundary conditions" within the Lattice-Boltzmann algorithm states that coupling between the fluid and cell occurs via the force

$$f = \xi(u - v) \tag{5}$$

where v is the velocity of a cell node, u is the average velocity of the neighbouring fluid nodes and ξ is a coupling coefficient set as 1.5 arbitrary units. The dynamics of a bacterial cell in a fluid is normally described as motion in a viscous molasses [32]. This is often called the Stokes regime and is normally identified by Reynolds numbers ranging from 10^{-6} to 10^{-3}. Hydrodynamic parameters in the current simulation were chosen to achieve a Reynolds number of 10^{-5}. With the choice of friction coefficient mentioned above and a Reynolds number of 10^{-5}, the velocity field of the fluid reaches values in the range of tens of micrometres per second.

The cellular mesh interacts with the substrate during the simulation, with the latter modelled as another triangular mesh. The employed substrate geometry was chosen to reflect the topography of laser-textured stainless-steel substrates that have been shown experimentally to reduce bacterial attachment for specific bacterial cells [28]. Two types of quasi-regular arrays comprising elongated ripples and isolated dots, respectively, were chosen for simulations. This choice of topography was based on the laser-textured surfaces shown in Fig. 3, which were produced with ultrashort laser pulses having linear and circular polarisation, respectively. In the former case, LIPSS formed perpendicular to the polarisation direction and resulted in elongated ridges. In the latter, the intersection of radial LIPSS forming perpendicular to the local polarisation orientation with successive overlapping laser pulses led to the formation of spikes or dots similar in dimensions to the laser wavelength. The period of the simulated arrays was taken as 0.30 μm for ripples and 1.50 μm for dots, respectively. Let (x,y,z) be the spatial coordinates of a generic node of the substrate mesh. To obtain a *quasi* dot-like triangular mesh, the following relationship between x, y and z was employed:

$$z(x,y) = A\left[\sin\left(\frac{2\pi}{\lambda_x}x\right)\sin\left(\frac{2\pi}{\lambda_y}y\right)\right]^2 \tag{6}$$

Elongated ripples were instead reproduced with the following relation:

$$z(x,y) = A\left[\sin\left(\frac{2\pi}{\lambda_x}x\right)\right]^2 \tag{7}$$

The code simulates non-covalent interactions between the cell and substrate in terms of two point forces generated on cell nodes by force centres corresponding to the substrate nodes. The interaction between a single cellular node i and a single substrate node j is simulated by the Lennard-Jones potential (see Fig. 2):

$$V(r_{ij}) = \varepsilon\left[\left(\frac{r_{min}}{r_{ij}}\right)^{12} - 2\left(\frac{r_{min}}{r_{ij}}\right)^{6}\right] \tag{8}$$

This potential is widely employed in MD simulations due to the fact that it effectively models surface interactions on a colloidal scale. Such interactions generally have a short range repulsive character, represented by the twelfth power term in Eq. (8), combined with long range attractive interactions, represented by the sixth power term. Parameters employed for simulations are summarised in Table 2.

Table 1
Bonding parameters in MD units relating to the simulations. All parameters are described in terms of three fundamental units: the unit of length corresponds to a physical length of 150 nm; the unit of time corresponds to a physical time interval of 10^{-3} s and the unit of mass corresponds to $1.55 * 10^{-19}$ kg.

Parameter	Value (MD units)
0	12
k_b	12
k_{al}	0.02
k_{ag}	0.9
k_v	1.5

3. Results and discussion

Fig. 4 shows a sequence of snapshots taken from the simulation of a spherical cell representing a coccoidal bacterium immersed in a fluid moving from left to right. For the sake of conciseness, we report only four snapshots for all simulated computational conditions. The cell interacts with a "dot-like" substrate based on the surface presented in Fig. 3(b), achieved through laser-texturing of stainless steel surfaces in a previous study [28]. Cellular motion induced by the fluid when the cell is not interacting with the substrate is mainly translational in nature, in agreement with the drag effect induced by the fluid. Owing to interaction between the cell and substrate, however, the cell shape deviates from its equilibrium spherical form and its kinetic energy

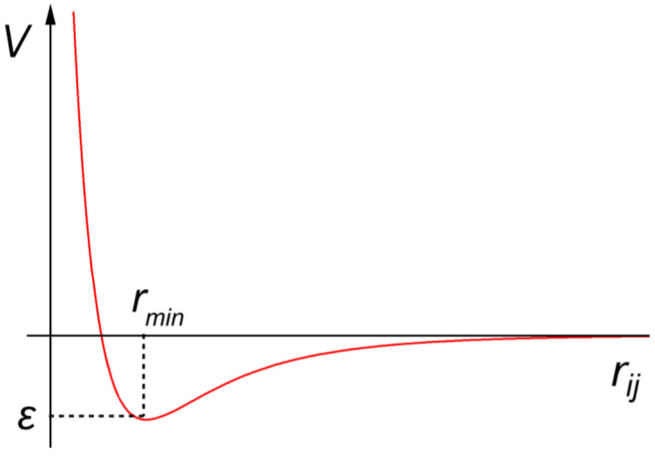

Fig. 2. Representation of the Lennard-Jones potential.

Table 2
Lennard-Jones parameters employed for simulations.

Parameter	Value
ε	3.5×10^{-28} J
r_{min}	33 nm

acquires a rotational component. The consequence is a decrease in the centre-of-mass velocity. After having interacted with the first dot-like protrusion, the cellular mesh essentially restores its spherical shape and maintains mostly translational motion approaching the top of subsequent protrusions without significant increases in its rotational kinetic energy.

The aforementioned behaviour is represented in Fig. 5, which reports the rotational energy and centre-of-mass velocity component in the direction of flow as functions of time. Both graphs show a repeated, quasi-periodic trend, reflecting the occurrence of "bounces" on top of substrate protrusions. The first bounce, in which interactions between the cellular mesh and substrate are maximum in strength, leads to a significant decrease in the centre-of-mass velocity and, correspondingly, to an increase in rotational energy. Since interactions between the cell and substrate are weaker in subsequent bounces, the effect becomes less evident.

These results highlight the role played by surface topography in dictating cell dynamics, a key finding of experimental works investigating the effect of ultrashort pulsed laser texturing on bacterial adhesion [8]. By changing the surface texture, cell dynamics are modified. Fig. 5 displays the corresponding behaviour of a cell interacting with "ripple-like" structures obtained by ultrashort pulsed laser texturing of stainless steel (Fig. 3(a)) [28] featuring a height similar to the previously considered dots but a smaller spatial period. In this case, the cell bounces more frequently but with a less pronounced overall decrease in centre-of-mass velocity due to the smaller surface feature height.

As far as cell-substrate interactions are concerned, it can be remarked that these are governed not only by the distance-dependent Lennard-Jones potentials presented in Eq. (8), but also by local hydrodynamic effects induced by the surface topography. This is supported by the simulated fluid velocity field represented by the coloured streamlines in Fig. 4. Under the simulated conditions and assuming a flat surface, the fluid velocity would be homogeneous throughout the entire volume with the exception of a very thin layer close to the surface where the fluid would be at rest. Both the surface topography and immersed cell produce local modifications in fluid velocity field. For instance, fluid velocity around the cell approaching the side wall of a protrusion increases, as shown by the red streamlines in Fig. 4(b). Local modifications in fluid velocity, in turn, affect cell dynamics, thus contributing to the levitation effect that makes the cell overcome the dot-like protrusion, together with the repulsive nature of the Lennard-Jones potential at short distance. In addition, cell deformation leading to deviations from a spherical shape also depends on the fluid velocity distribution.

In the case of ripples, the cell spends a comparatively small amount of time between adjacent protrusions, where the fluid velocity field is more markedly modified. As a consequence, shape deformations are less pronounced, leading to smaller contributions from rotational degrees of freedom to the overall kinetic energy (see Fig. 6(b)).

The simulations clearly address the initial stages of bacterial attachment prior to the onset of any chemical or biological effects that would eventually lead to irreversible adhesion. Treatment of these factors would require detailed knowledge of the chemical properties of the fluid and surface, and a model for the vital activity of the selected bacterial cells.

Nonetheless, the length of time a cell spends in proximity to a surface can be expected to heavily affect attachment of single bacterial cells and subsequent biofilm formation. These results suggest that textures with large "hills" will increase the stay time in between adjacent protrusions. The related phenomenon is known in the literature as the "shelter" effect [21] where the surface roughness acts as a shelter that protects a bacterial cell from hydrodynamic turbulence.

Conversely, stay time may decrease with higher density, smaller surface structures. This observation was confirmed by conducting additional simulations, presented as an example in Fig. 7, with textures having the same spatial period as the previously-considered dots but with higher peaks. Though structures with a large aspect ratio are usually not achieved via single-pass ultrashort pulsed laser machining, they can be envisioned within presently available surface processing methods.

Snapshots shown in Fig. 7 demonstrate strong deformation of the cell caused by prolonged interaction with the rigid wall of the protrusion. In such conditions, the centre-of-mass velocity is markedly reduced compared to flow above a flat surface, eventually leading the bacterium to stop completely. In such conditions, adhesion is expected to be favoured as the substrate effectively behaves as a bacterial trap.

Fig. 8 shows a graph of the stay time, measured as the time required for the cell to reach the top of a single dot-like protrusion, as a function of the aspect ratio of the protrusion, defined as the ratio between the height and the period of the dot-like pattern. The latter was fixed at 1500 nm in all cases.

The graph shows that the cell stays in proximity to the surface for a time interval that increases with the height of the protrusions, achieving asymptotic behaviour for an aspect ratio of 0.55. This corresponds to a height of 825 nm. The significance of this result is that the threshold height is comparable to the cell size of 600 nm. The simulation therefore confirms that the cell size establishes an upper critical threshold for the size of protrusions for surfaces that must exhibit negligible shelter effect.

Though existing theory relating to the initial phases of bacterial attachment essentially considers the relationship between the bacterial

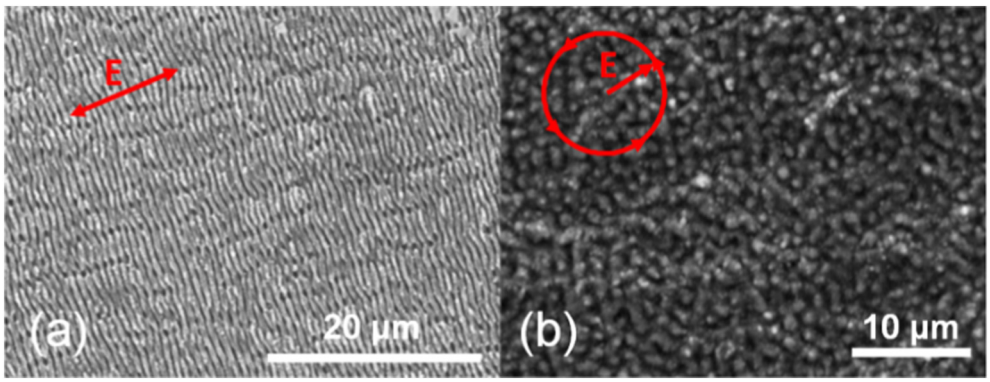

Fig. 3. SEM images of ripples perpendicular to the light polarisation (red arrow) (a) and dots produced with circular polarisation (b). Ripples are elongated ridge-like protrusions with typical periods of 0.7–0.8 μm. Dots occur as bump-like structures with a typical diameter of ~1 μm. (For interpretation of the references to colour in this figure legend, the reader is referred to the web version of this article.)

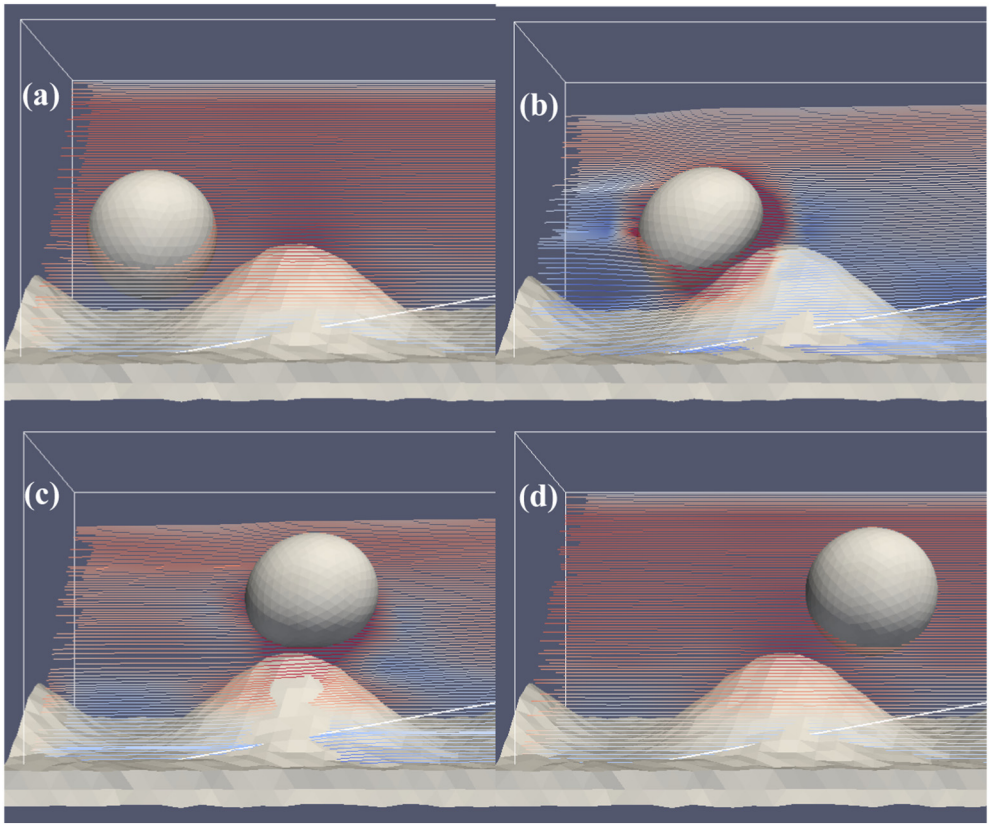

Fig. 4. Snapshots showing the behaviour of a single coccoidal bacterium near a "dot-like" surface [12] at consecutive points in time: 0.1 ms (a); 0.3 ms (b); 0.5 ms (c); 0.7 ms (d). The fluid velocity field is shown as streamline colours from blue to red for increasing velocity. (For interpretation of the references to colour in this figure legend, the reader is referred to the web version of this article.)

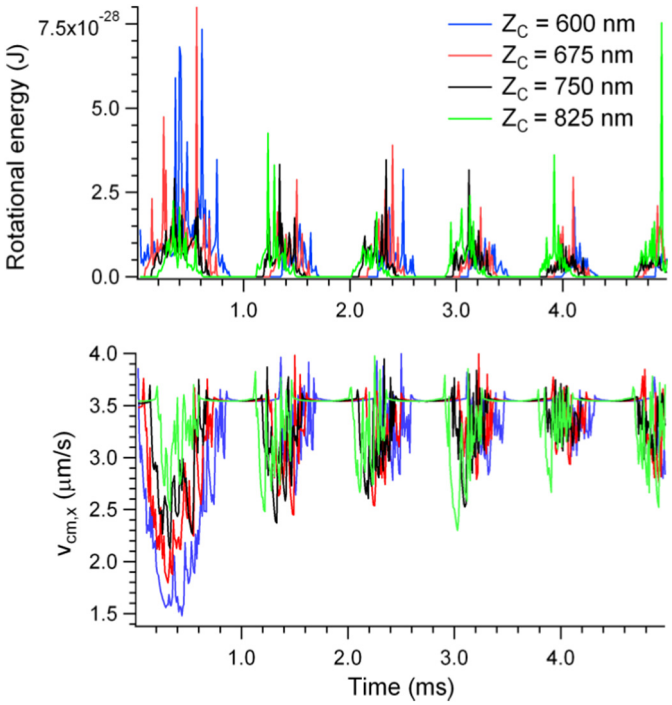

Fig. 5. Rotational energy (a) and centre-of-mass velocity $v_{cm,\ x}$ (b) along the flow direction vs. time for a single spherical mesh moving in proximity to a dot-like surface. Z_c represents the initial height of the cell from the substrate. The spikes are the result of numerical effects due to the discrete nature of the simulation procedure.

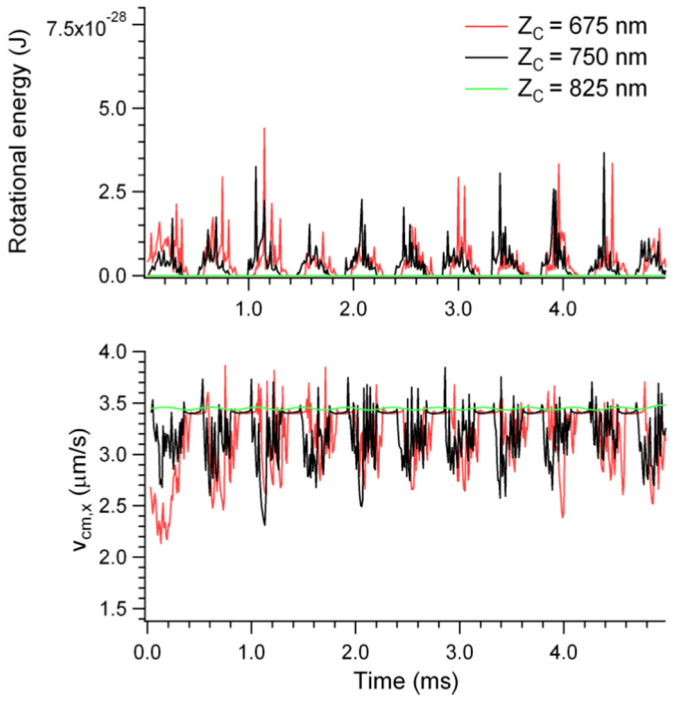

Fig. 6. Rotational energy (a) and centre-of-mass velocity $v_{c\ m,\ x}$ (b) along the flow direction vs. time for a single spherical mesh moving in proximity to a ripple-like surface. Z_c represents the initial height of the cell from the substrate. The spikes are the result of numerical effects due to the discrete nature of the simulation procedure.

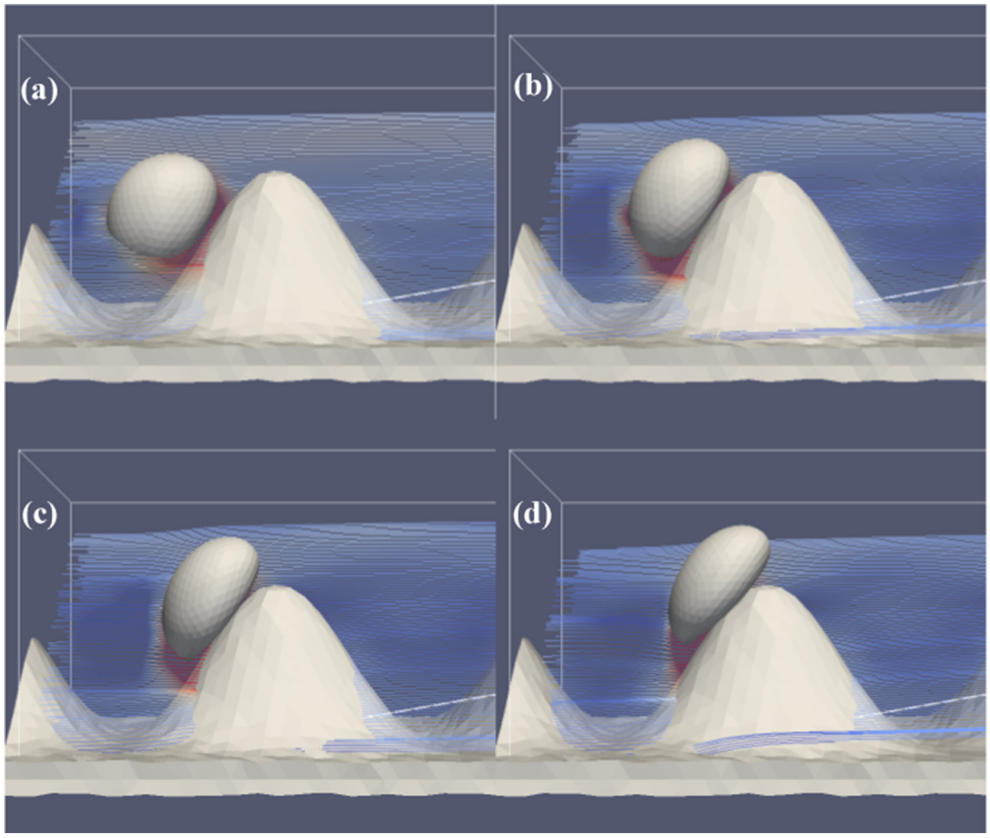

Fig. 7. Snapshots showing the behaviour of a single coccoidal bacterium at consecutive points in time near a "dot-like" surface with higher protrusions than in Fig. 2: 0.1 ms (a); 0.3 ms (b); 0.5 ms (c); 0.7 ms (d). It should be noted that the increase in height leads to larger deformation of the cellular mesh and a larger contact area. This should lead to an increase in the probability of adhesion.

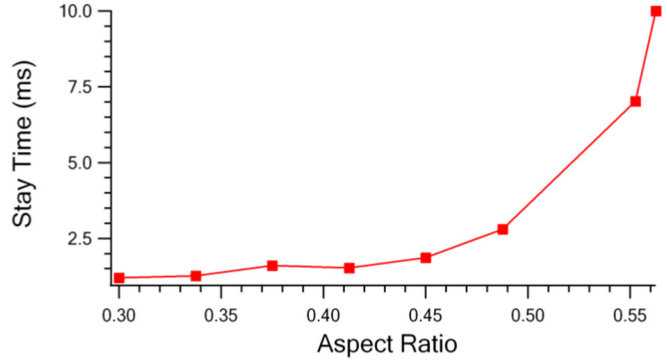

Fig. 8. Stay time vs. aspect ratio for a cell in proximity to a dot-like protrusion (λ_x = 1500 nm).

cell size and surface feature dimensions in terms of attachment point theory [33,34], simulation results presented here within suggest a more complex scenario involving the interaction between a cell and substrate in the presence of important hydrodynamic turbulence. While the number of available contact points for bacterial cells is expected to decrease with surface features smaller than the cell size, reductions in bacterial attachment approaching this point [35] are likely due to more complex effects. Simulation results therefore have important implications for the design and production of antibacterial surfaces, providing a clear methodology and guidelines for topography appropriate for reducing bacterial attachment.

4. Conclusion

By analyzing observables related to the motion and the interactions between a single spherical cell and a substrate inspired to laser textured surfaces, we observed the so-called "shelter effect" in terms of an increase in the stay time of a factor ~4 for topographies whose size are larger than the cellular size. The experimental textures to which the computational surfaces are inspired are considered good candidates for achieving antibacterial behaviour, since they show values of areal surface roughness compatible with the requirements for an antibacterial behaviour (S_a = (90 ± 5) nm for the ripples, S_a = (60 ± 5) nm for the dots). Simulation of the interaction between a bacterial cell and textured substrate allows the biological response of a metal surface to be tuned, opening up new possibilities for the design and manufacture of components that are strongly resistant to biofouling. The model presented within this work represents a step forward in developing reliable laser-based manufacturing methods for improving the antibacterial performance of surfaces. Though such processes have been demonstrated empirically in the past, their optimisation has not been possible due to lack of a detailed and comprehensive approach taking into account the mechanisms of bacterial adhesion at the scale of surface roughness.

In relation to the two laser-textured surfaces considered in this work, the following conclusions can be drawn:

- The motion of a cell immersed in a fluid in proximity to a textured surface is strongly influenced by surface topography;
- Surface protrusions present on textured substrates act as obstacles that lower the cell velocity, extending the stay time inside the region between two adjacent surface protrusions and therefore the probability of irreversible adhesion;
- The hypotheses relating to the influence of surface topography on bacterial adhesion has been confirmed with simulation data, in particular in relation to the "shelter" effect discussed in the literature;
- Conversely, the model suggests that in the presence of densely packed surface structures such as those on laser-textured antibacterial surfaces, a single bacterial cell tends to be completely exposed to hydrodynamic turbulence and is therefore less prone to

adhere to the surface itself.

The next phase of model development will include accounting for different bacteria shapes and specific surface parameters such as peak form, height, period and density in order to establish the ideal topography to inhibit the initial stages of bacterial adhesion and allow appropriate process parameters to be selected for their production. Bacterial adhesion involves a plethora of different mechanisms, for which the influence of the specific bacterial strain, interactions between neighbouring bacterial cells and the presence of proteic waste materials filling the space between surface protrusions must be investigated. These aspects, together with industrial considerations such as the lifetime of processed surfaces subject to wear or chemical corrosion, will be the object of future investigations.

Acknowledgments

This work has received funding from the EU Horizon 2020 Research and Innovation Programme under Grant Agreement No 687613. This research also benefited from the HPC (High Performance Computing) facility at the University of Parma, Italy.

References

[1] J.S. Price, A.F. Tencer, D.M. Arm, G.A. Bohach, Controlled release of antibiotics from coated orthopedic implants, J. Biomed. Mater. Res. 30 (1996) 281–286, https://doi.org/10.1002/(SICI)1097-4636(199603)30:3%3C281::AID-JBM2%3E3.0.CO;2-M.
[2] L. Zhao, P.K. Chu, Y. Zhang, Z. Wu, Antibacterial coatings on titanium implants, J. Biomed. Mater. Res., Part B 91 (2009) 470–480. 10.1002/jbm.b.31463[4] A.J.
[3] A.J. Tande, R. Patel, Prosthetic joint infection, Clin. Microbiol. Rev. 27 (2014) 302–345, https://doi.org/10.1128/CMR.00111-13.
[4] S. Srey, I.K. Jahid, S. Ha, Biofilm formation in food industries: a food safety concern, Food Control 31 (2013) 572–585, https://doi.org/10.1016/j.foodcont.2012.12.001.
[5] M.V. Graham, N.C. Cady, Nano and microscale topographies for the prevention of bacterial surface fouling, Coatings 4 (2014) 37–59, https://doi.org/10.3390/coatings4010037.
[6] Y. Ammar, D. Swailes, B. Bridgens, J. Chen, Influence of surface roughness on the initial formation of biofilm, Surf. Coat. Technol. 284 (2015) 410–416, https://doi.org/10.1016/j.surfcoat.2015.07.062.
[7] X. He, Y. Liu, Y. Gong, C. Zhou, H. Li, Autoclaving-induced in-situ grown alumina on arc-sprayed aluminum coatings: multiscaled topography facilitates antifouling performances, Surf. Coat. Technol. 309 (2017) 295–300, https://doi.org/10.1016/j.surfcoat.2016.11.066.
[8] A.H.A. Lutey, L. Gemini, L. Romoli, G. Lazzini, F. Fuso, M. Faucon, R. Kling, Towards laser-textured antibacterial surfaces, Sci. Rep. 8 (2018) 10112, https://doi.org/10.1038/s41598-018-28454-2.
[9] G.R.B.E. Römer, A.J. Huis, J. Meijer, M.N.W. Groenendijk, On the formation of laser induced self-organizing nanostructures, CIRP Ann-Manuf. Techn. 58 (2009) 201–204, https://doi.org/10.1016/j.cirp.2009.03.068.
[10] L. Romoli, C.A.A. Rashed, G. Lovicu, G. Dini, F. Tantussi, F. Fuso, M. Fiaschi, Ultrashort pulsed laser drilling and surface structuring of microholes in stainless steels, CIRP Ann-Manuf. Techn. 63 (2014) 229–232, https://doi.org/10.1016/j.cirp.2014.03.053.
[11] D.M. Chun, C.V. Ngo, K.M. Lee, Fast fabrication of superhydrophobic metallic surface using nanosecond laser texturing and low-temperature annealing, CIRP Ann. Manuf. Technol. 65 (2016) 519–522, https://doi.org/10.1016/j.cirp.2016.04.019.
[12] D.R. Sierra, S.P. Edwardson, G. Dearden, Laser surface texturing of titanium with thermal post-processing for improved wettability properties, Proc. CIRP 74 (2018) 362–366, https://doi.org/10.1016/j.procir.2018.08.143.
[13] O. El-Atwani, S. Gonderman, A. DeMasi, A. Suslova, J. Fowler, M. El-Atwani, K. Ludwig, J.P. Allain, Nanopatterning of metal-coated silicon surfaces via ion beam irradiation: real time X-ray studies reveal the effect of silicide bonding, J. Appl. Phys. 113 (2013) 124305, , https://doi.org/10.1063/1.4797480.
[14] I. Gnilitskyi, T.J.-Y. Derrien, Y. Levy, N.M. Bulgakova, T. Mocek, L. Orazi, High-speed manufacturing of highly regular femtosecond laser-induced periodic surface structures: physical origin of regularity, Sci. Rep. 7 (2017) 8485, https://doi.org/10.1038/s41598-017-08788-z.
[15] N. Grossman, E.Z. Ron, C.L. Woldringh, Changes in cell dimensions during amino acid starvation of Escherichia coli, J. Bacteriol. 152 (1982) 35.
[16] P.J. Wyatt, Cell wall thickness, size distribution, refractive index ratio and dry weight content of living bacteria (Staphylococcus aureus), Nature 226 (1970) 277.
[17] A. Rosenkranz, M. Hans, C. Gachot, A. Thome, S. Bonk, F. Mücklich, Direct laser interference patterning: tailoring of contact area for frictional and antibacterial properties, Lubricants 4 (2016) 2, https://doi.org/10.3390/lubricants4010002.
[18] J. Valle, S. Burgui, D. Langheinrich, C. Gil, C. Solano, A. Toledo-Arana, R. Helbig, A. Lasagni, I. Lasa, Evaluation of surface microtopography engineered by direct laser interference for bacterial anti-biofouling, Macromol. Biosci. 15 (2015) 1060–1069, https://doi.org/10.1002/mabi.201500107.
[19] S. Hammouti, B. Holybee, W. Zhu, J.P. Allain, B. Jurczyk, D. Ruzic, Titanium nitride formation by a dual-stage femtosecond laser process, Appl. Phys. A Mater. Sci. Process. 124 (2018) 411.
[20] C. Berne, C.K. Ellison, A. Ducret, Y.V. Brun, Bacterial adhesion at the single-cell level, Nat. Rev. Microbiol. 16 (2018) 616–627, https://doi.org/10.1038/s41579-018-0057-5.
[21] V.K. Truong, H.K. Webb, E. Fadeeva, B.N. Chichkov, A.H.F. Wu, R. Lamb, J.Y. Wang, R.J. Crawford, E.P. Ivanova, Air-directed attachment of coccoid bacteria to the surface of superhydrophobic lotus-like titanium, Biofouling 28 (2012) 539–550, https://doi.org/10.1080/08927014.2012.694426.
[22] Y. Liu, J. Strauss, T.A. Camesano, Adhesion forces between Staphylococcus epidermidis and surfaces bearing self-assembled monolayers in the presence of model proteins, Biomaterials 29 (2008) 4374–4382, https://doi.org/10.1016/j.biomaterials.2008.07.044.
[23] C. Jullien, T. Bénézech, B. Carpentier, V. Lebret, C. Faille, Identification of surface characteristics relevant to the hygienic status of stainless steel for the food industry, J. Food Eng. 56 (2003) 77–87, https://doi.org/10.1016/S0260-8774(02)00150-4.
[24] C.M. Bollenl, P. Lambrechts, M. Quirynen, Comparison of surface roughness of oral hard materials to the threshold surface roughness for bacterial plaque retention: a review of the literature, Dent. Mater. 13 (1997) 258–269.
[25] G.S. Watson, D.W. Green, L. Schwarzkopf, X. Li, B.W. Cribb, S. Myhra, J.A. Watson, A gecko skin micro/nano structure–a low adhesion, superhydrophobic, anti-wetting, self-cleaning, biocompatible, antibacterial surface, Acta Biomater. 21 (2015) 109–122, https://doi.org/10.1016/j.actbio.2015.03.007.
[26] E.P. Ivanova, J. Hasan, H.K. Webb, V.K. Truong, G.S. Watson, J.A. Watson, V.A. Baulin, S. Pogodin, J.Y. Wang, M.J. Tobin, C. Löbbe, R.J. Crawford, Natural bactericidal surfaces: mechanical rupture of Pseudomonas aeruginosa cells by cicada wings, Small 8 (2012) 2489–2494, https://doi.org/10.1002/smll.201200528.
[27] M.J. Hayes, T.P. Levine, R.H. Wilson, Identification of nanopillars on the cuticle of the aquatic larvae of the drone fly (Diptera: Syrphidae), J. Insect Sci. 16 (2016) 1–7, https://doi.org/10.1093/jisesa/iew019.
[28] L. Romoli, F. Tantussi, F. Fuso, Laser milling of martensitic stainless steels using spiral trajectories, Opt. Lasers Eng. 91 (2017) 160–168, https://doi.org/10.1016/j.optlaseng.2016.11.016.
[29] I. Cimrak, M. Gusenbauer, I. Jančigová, An ESPResSo implementation of elastic objects immersed in a fluid, Comput. Phys. Commun. 185 (2014) 900–907, https://doi.org/10.1016/j.cpc.2013.12.013.
[30] H.J. Limbach, A. Arnold, B.A. Mann, C. Holm, C, ESPResSo—an extensible simulation package for research on soft matter systems, Comput. Phys. Commun. 174 (2006) 704–727, https://doi.org/10.1016/j.cpc.2005.10.005.
[31] R.G. Bailey, R.D. Turner, N. Mullin, N. Clarke, S.J. Foster, J.K. Hobbs, The interplay between cell wall mechanical properties and the cell cycle in Staphylococcus aureus, Biophys. J. 107 (2014) 2538–2545, https://doi.org/10.1016/j.bpj.2014.10.036.
[32] A. Persat, C.D. Nadell, M.K. Kim, F. Ingremeau, A. Siryaporn, K. Drescher, N.S. Wingren, B.L. Bassler, Z. Gitai, H.A. Stone, The mechanical world of bacteria, Cell 161 (2015) 988–997, https://doi.org/10.1016/j.cell.2015.05.005.
[33] A.J. Scardino, J. Guenther, R. de Nys, Attachment point theory revisited: the fouling response to a microtextured matrix, Biofouling 24 (2008) 45–53, https://doi.org/10.1080/08927010701784391.
[34] K.A. Whitehead, J. Verran, The effect of surface topography on the retention of microorganisms, Food Bioprod. Process. 84 (2006) 253–259, https://doi.org/10.1205/fbp06035.
[35] N. Lu, W. Zhang, Y. Weng, X. Chen, Y. Cheng, P. Zhou, Fabrication of PDMS surfaces with micro patterns and the effect of pattern sizes on bacteria adhesion, Food Control 68 (2016) 344–351, https://doi.org/10.1016/j.foodcont.2016.04.014.